Propagation of whistler mode waves with a modulated frequency in the magnetosphere

A. V. Streltsov,[1] M. Gołkowski,[2] U. S. Inan,[3] and K. D. Papadopoulos[4]

Received 2 December 2009; revised 10 March 2010; accepted 16 March 2010; published 10 September 2010.

[1] This paper presents results from experimental and numerical studies of the propagation of whistler mode waves in the Earth's magnetosphere. An experiment conducted at the High Frequency Active Auroral Research Program (HAARP) on 16 March 2008 demonstrates that ionospherically generated waves with particular frequency-time formats are amplified on their pass from HAARP to the conjugate location in the South Pacific Ocean more efficiently than waves with a constant frequency. Numerical simulations of a one-dimensional electron magnetohydrodynamics (MHD) model in the dipole magnetic field geometry reveal that the amplification takes place more efficiently when the frequency of the whistler mode waves (in the frequency range from 0.5 to 1.0 kHz) changes in the equatorial magnetosphere with the rate from 0.25 to 0.47 kHz/s. The maximum amplification occurs when this rate is 0.33 kHz/s and no/very little amplification is observed when this gradient is equal to 0 or when it is larger than 0.78 kHz/s.

Citation: Streltsov, A. V., M. Gołkowski, U. S. Inan, and K. D. Papadopoulos (2010), Propagation of whistler mode waves with a modulated frequency in the magnetosphere, *J. Geophys. Res.*, *115*, A09209, doi:10.1029/2009JA015155.

1. Introduction

[2] The propagation and amplification of VLF whistler mode waves in the magnetosphere have been studied for more than 3 decades. One of the main reasons for interest in the dynamics of these waves is their ability to interact efficiently viacyclotron resonance with energetic electrons in the magnetosphere [*Nunn*, 1974; *Karpman et al.*, 1974; *Omura et al.*, 1991; *Trakhtengerts et al.*, 1996; *Nunn and Smith*, 1996; *Hobara et al.*, 2000; *Trakhtengerts and Rycroft*, 2008]. These interactions can change the pitch angle of the energetic particles and precipitate them into the ionosphere. Therefore, controlled injection of whistlers into the magnetosphere can decrease the number of energetic particles inside the Earth's radiation belts and make the radiation environment safer for spacecraft [*Inan et al.*, 2003].

[3] The same wave-particle interactions also lead to a nonlinear amplification of whistler mode waves and to generation of intense secondary emissions. Although such an amplification of the initial (triggering) signal and the generation of secondary emissions have been observed in a number of experiments conducted at Siple Station in Antarctica [*Helliwell et al.*, 1980; *Inan et al.*, 1985; *Helliwell*, 1988; *Helliwell et al.*, 1990] and a number of theoretical/numerical studies have been devoted to this problem, the definitive answer to the question of what parameters of the initial whistler mode wave cause amplification/triggering/particle precipitation in different geophysical conditions has not yet been satisfactorily answered.

[4] One reason for uncertainty is that wave-particle interactions leading to these nonlinear effects can occur in a large volume of the equatorial magnetosphere, where the parameters of the background plasma and the triggering wave are (1) not defined well and (2) changing in space along the wave trajectory. Another complexity to the problem is added by the fact that these interactions are nonlinear, and they depend on the wave amplitude and density of the energetic particles. Therefore, even a comprehensive theoretical analysis of the linearized system of wave-particle equations or nonlinear equations in a homogeneous background magnetic field and plasma do not provide a quantitative understanding of the problem that can be used to predict results from quite sophisticated and expensive future experiments. The only way to develop such understanding is by using multidimensional numerical models describing whistler mode wave propagation and interaction between these waves and energetic electrons in a realistic geospace environment. The results from these modeling studies should be compared with observations. This paper presents results from a detailed, numerical study of the propagation of whistler mode waves transmitted by the High Frequency Active Aurora Research Program (HAARP) facility in Gakona, Alaska.

[1]Thayer School of Engineering, Dartmouth College, Hanover, New Hampshire, USA.
[2]Department of Electrical Engineering, University of Colorado, Denver, Colorado, USA.
[3]STAR Laboratory, Stanford University, Stanford, California, USA.
[4]Department of Physics and Astronomy, University of Maryland, College Park, Maryland, USA.

0148-0227/10/2009JA015155

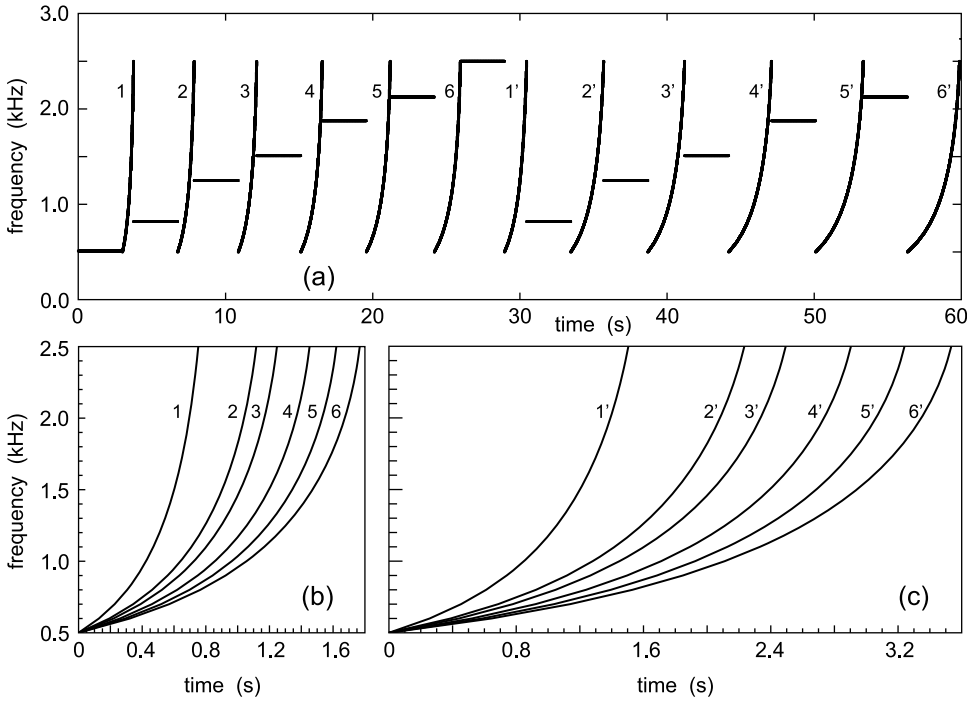

Figure 1. Temporal frequency variations of whistler mode waves transmitted by HAARP on 16 March 2008. (a) The format as it was transmitted. (b and c) Detailed views of the frequency-time signatures contained in the format.

The HAARP facility is an ionospheric heater that is able to generate extremely low frequency (ELF)/very low frequency (VLF) waves by modulating the ionospheric conductivity in the *D* region and thus modify the auroral electrojet currents [*Papadopoulos et al.*, 2003; *Gołkowski et al.*, 2008; *Cohen et al.*, 2008]. In the absence of conventional transmitters in the ELF/VLF: 500 Hz to 8 kHz band (Siple Station was discontinued in 1988), HAARP provides a unique platform for controlled wave injection studies.

2. HAARP Experiment

[5] The HAARP facility is located at ~62.4°N and 145.2°W geographic (63.1°N and 92.4°W geomagnetic). The HF heater consists of 180 crossed dipoles arranged in a 12 × 15 rectangular array capable of a total radiated power of 3.6 MW and effective radiated power (ERP) of ~575 MW. During an experiment on 16 March 2008 HAARP transmitted in the X mode using a 2.75 MHz carrier frequency. Whistler mode waves with frequency changing in time from 0.5 to 2.5 kHz as well as constant frequency pulses at 510, 820, 1250, 1510, 1875, 2125, and 2500 Hz were generated. Figure 1a shows the 60 s format that was repeated for 30 min from 22:30 to 23:00 UT. Figures 1b and 1c show detailed views of the special frequency-time signatures contained in the transmission format and labeled 1, 2, 3, 4, 5, 6 and 1′, 2′, 3′, 4′, 5′, 6′. The signals in Figure 1c (1′, 2′, 3′, 4′, 5′, 6′) differ from the corresponding signals in Figure 1b (1, 2, 3, 4, 5, 6) by a factor of 2 dilation in time. Ground measurements of ELF/VLF waves were made in the vicinity of the HAARP facility at Chistochina, Alaska, and also in the magnetic conjugate region in the South Pacific Ocean onboard the research ship *Tangaroa*. Table 1 shows the geographic coordinates and geomagnetic *L* parameters of HAARP, its conjugate point, and there ceiving stations. The *L* parameters and conjugate location shown in Table 1 were derived using an IGRF model of the the geomagnetic field at 80 km altitude. The ELF/VLF receivers used are Stanford Atmospheric Weather Educational System for Observation and Modeling of Effects (AWESOME) receivers and utilize large square (4.8 m × 4.8 m) or triangular (4.2 m high with a 8.4 m base) air core antennas, with terminal resistive and inductive impedances, respectively, of 1 Ω and 1 mH, matched to a low-noise (noise figure of ~2–3 dB at a few kHz) preamplifier with a flat frequency response (~300 Hz to ~40 kHz). The receiver hardware is described in detail by *Cohen et al.* [2010]. A more detailed description of the HAARP wave injection experiment is provided by *Gołkowski et al.* [2008].

3. Observations

[6] Figure 2 (top) shows spectrograms of the signals measured at Chistochina corresponding to the first 30 s of the transmission format when the six signals (1, 2, 3, 4, 5, 6) with frequency changing in time shown in Figure 1b were

Table 1. Locations of HAARP and Ground Receivers

Site	Latitude	Longitude	*L* Shell
HAARP	62.39°N	145.15°W	4.93
Chistochina	62.61°N	144.62°W	5.05
HAARP Conj. Point	56.67°S	174.50°E	4.93
Tangaroa	60.01°S	172.15°E	6.55

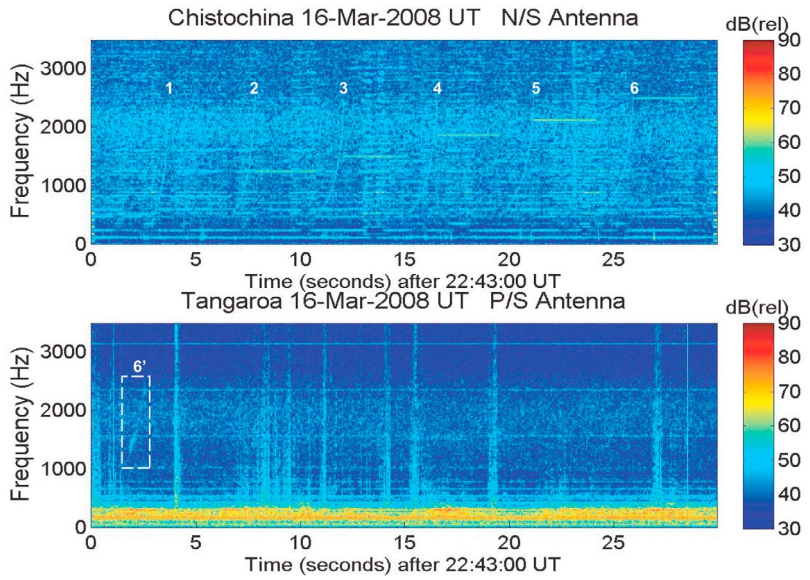

Figure 2. (Top) Spectrogram of the signal measured near the HAARP site (at Chistochina) on 16 March 2008. (Bottom) Spectrogram of the signal measured by the research ship *Tangaroa* at the magnetically conjugate to HAARP point in southern Pacific Ocean.

transmitted. Figure 2 (bottom) shows the spectrogram of the signal received on *Tangaroa* in the conjugate region. No amplification of these signals (or any transmitted signals) was detected during this part of the experiment.

[7] Figure 3 (top) shows spectrograms of the signals observed at Chistochina, Alaska, during the second 30 s of the transmission format, when the six signals (1′, 2′, 3′, 4′, 5′, 6′) with frequency changing in time shown in Figure 1c were transmitted. Figure 3 (bottom) shows the spectrogram of the signal received on the ship. In this experiment, a noticeable amplification of the signals with frequency modulations of types 2′, 3′, 4′, and 5′ was detected. The signal 6′ was also amplified, and this amplification is shown in Figure 2 (bottom). The amplified version of signal 6′ appears in Figure 2 because of the 1 min format repetition period and the ~2.5 s propagation time between the hemispheres. Therefore, the mark on the spectrogram in Figure 2 (bottom) near 22:43:02 UT (inside the dashed box) is the amplified signal with the 6′ frequency-time format transmitted by HAARP during the previous 1 min of the

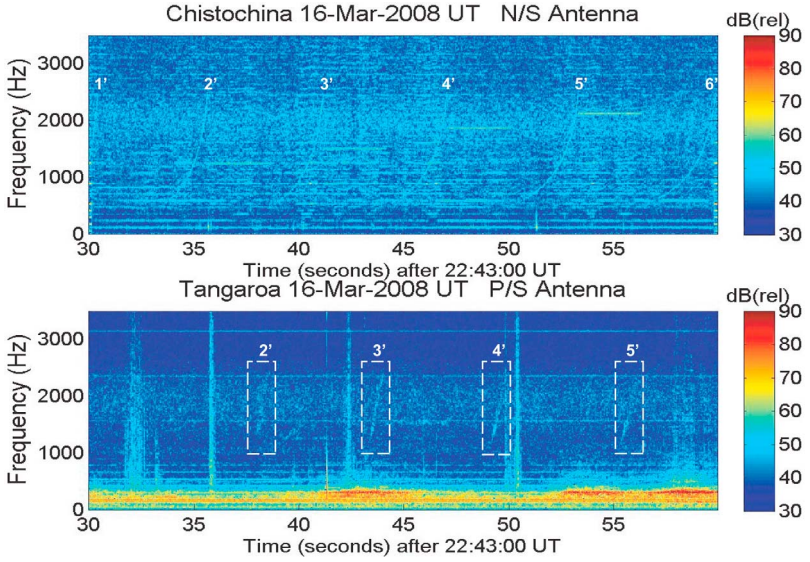

Figure 3. (Top) Spectrogram of the signal measured near the HAARP site. (Bottom) Spectrogram of the signal measured at the magnetically conjugate to HAARP point.

experiment. Although at the time of the observations *Tangaroa* was south of the HAARP conjugate point at a higher L shell than HAARP (see Table 1), it is assumed that the signals traversed the magnetosphere on L shells close to that of the HAARP facility as was found in previous HAARP wave injection experiments [*Inan et al.*, 2004; *Gołkowski et al.*, 2008, 2009, 2010].

[8] It is worth mentioning that during this experiment observations exhibited very little amplification of signals with constant frequencies in the range from 1.2 to 2.5 kHz, which were also launched during the same 1 min time intervals: Only two pulses with frequencies of 1250 and 1510 Hz were observed in the conjugate region and can be seen faintly around 39 and 44 s in Figure 3 (bottom). Therefore, results from the experiment conducted at HAARP on 16 March 2008 suggest that amplification of whistler mode waves is sensitive to the frequency-time format of the signals transmitted by ground-based transmitters. To answer the question under what conditions this amplification is possible, numerical simulations of the whistler propagation in the magnetosphere were performed.

4. Model

[9] Propagation of whistler mode waves along $L = 4.9$ magnetic field line has been modeled with a numerical algorithm based on one-dimensional (waves propagate only along $\mathbf{B}_0$) equations of electron magnetohydrodynamics (EMHD). The EMHD assumes that ions are immobile and electrons are treated as a cold fluid carrying current [*Helliwell*, 1965; *Gordeev et al.*, 1994]. The model consists of the electron momentum equation and Maxwell's equations. In this study, the displacement current in Ampere's law is neglected. This is a "quasi-longitudinal" approximation of EMHD, which is valid when the wave circular frequency ω satisfies conditions $\omega_{\mathrm{HL}} < \omega < \omega_{\mathrm{ce}} \ll \omega_{\mathrm{pe}}$ [*Sazhin*, 1993]. Here ω_{HL} is the lower hybrid frequency; ω_{ce} is the electron gyrofrequency; and ω_{pe} is the electron plasma frequency.

$$\frac{\partial \mathbf{v}}{\partial t} + (\mathbf{v}\cdot\nabla)\mathbf{v} = -\frac{e}{m_e}(\mathbf{E} + \mathbf{v}\times\mathbf{B}), \tag{1}$$

$$\nabla\times\mathbf{B} = \mu_0\mathbf{j}, \tag{2}$$

$$\nabla\times\mathbf{E} = -\frac{\partial \mathbf{B}}{\partial t}, \tag{3}$$

$$\nabla\cdot\mathbf{B} = 0. \tag{4}$$

[10] In the homogeneous case, equations (1)–(4) lead to a dispersion relation connecting wave frequency, ω, and the parallel wave number, $k_\parallel$, as

$$\omega = \frac{\omega_{\mathrm{ce}}}{\left(1 + \omega_{\mathrm{pe}}^2/c^2k_\parallel^2\right)}, \tag{5}$$

where ω_{pe} is the electron plasma frequency and ω_{ce} is the electron gyro frequency, with both varying along the magnetic field line with n and B_0, respectively. Relation (5) gives the following expression for the parallel group velocity

$$v_{\parallel g} = \frac{d\omega}{dk_\parallel} = \frac{2k_\parallel\omega_{\mathrm{ce}}\omega_{\mathrm{pe}}^2/c^2}{\left(k_\parallel^2 + \omega_{\mathrm{pe}}^2/c^2\right)^2}. \tag{6}$$

[11] Using relation $\mathbf{j} = -en_e\mathbf{v}$, equations (1)–(4) can be reduced to three vector equations for the wave magnetic field, $\mathbf{B}$, the electron fluid velocity, $\mathbf{v}$, and the electric field, $\mathbf{E}$,

$$\frac{\partial \mathbf{B}}{\partial t} = -\nabla\times\mathbf{E}, \tag{7}$$

$$\mathbf{v} = -\frac{1}{\mu_0 ne}\nabla\times\mathbf{B}, \tag{8}$$

$$\frac{m_e}{\mu_0 ne^2}\nabla\times\nabla\times\mathbf{E} + \mathbf{E} = -\frac{m_e}{e}(\mathbf{v}\cdot\nabla)\mathbf{v} - \mathbf{v}\times\mathbf{B}, \tag{9}$$

Equations (7)–(9) are solved numerically in the dipole orthogonal coordinates (shown in Figure 1 in *Streltsov et al.* [2009]), where the z axis is directed along the ambient magnetic field; the x axis lies in the meridional plane and is directed perpendicular to $\mathbf{z}$, toward the center of the Earth; and the y axis completes the right-hand coordinate system (x, y, z). This coordinate system adequately represents the ambient magnetic field starting in the ionosphere at the HAARP latitude.

[12] In this study, we consider the propagation of whistler mode waves in one spatial direction only (1D), namely along the ambient magnetic field. This type of propagation can happen when the wave is guided by the field-aligned density inhomogeneity or duct. Whistler mode waves in ducts have been observed in the Earth's magnetosphere [*Angerami*, 1970; *Scarf and Chapell*, 1973; *Carpenter and Anderson*, 1992; *Koons*, 1989; *Moullard et al.*, 2002] and in laboratory plasma devices [*Stenzel*, 1976; *Kostrov et al.*, 2000]. Therefore, the 1D case considered in this study is quite relevant to the whistler mode wave propagation in the real magnetosphere.

4.1. Background Parameters

[13] To execute simulations, parameters of the background plasma density and the ambient magnetic field should be established. We assume that the ambient magnetic field along $L = 4.9$ magnetic field line is close to that of a dipole. Therefore, we define $B_0 = B_*\ (1 + 3\ \sin^2\ \theta)^{1/2}/r^3$, where $B_* = 31000$ nT, θ is a colatitudinal angle, and r is a geocentric distance measured in $R_E = 6371.2$ km.

[14] To define the density distribution several assumptions have been made. First, we assume a parametric form of the dependency of the density on the radial distance in the magnetosphere. One such form is given by *Streltsov et al.* [2009]; another, which is used in this study, is

$$n(r) = \begin{cases} a_1(r - r_2) + a_2, & r_1 < r < r_2 \\ b_1 e^{-(r-r_2)/r_0} + b_2 r^{-\gamma}, & r > r_2 \end{cases}. \tag{10}$$

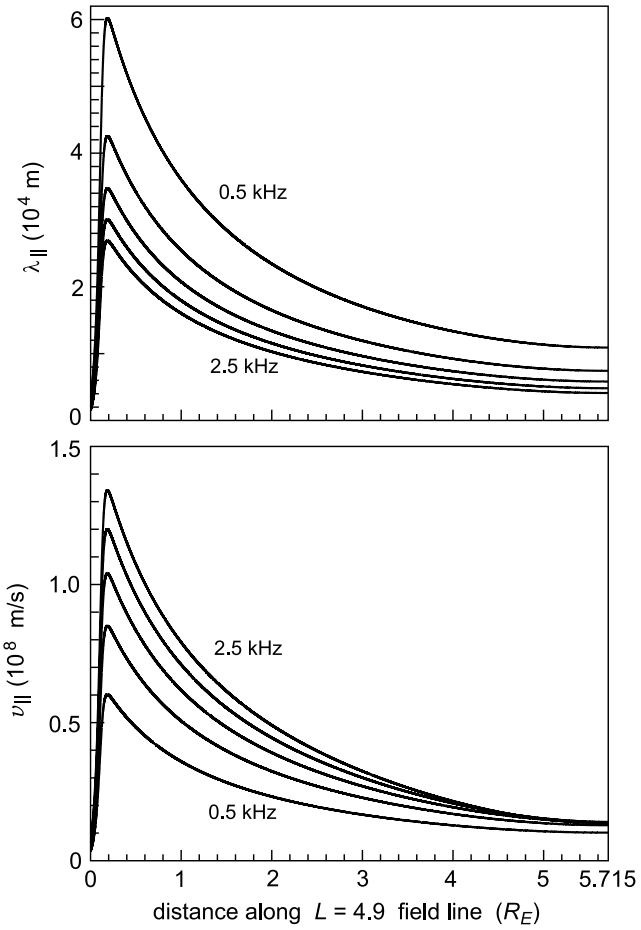

Figure 4. Parallel wavelength (top) and the parallel group velocity (bottom) of the whistler mode waves with frequencies 0.5, 1, 1.5, 2, and 2.5 kHz along $L = 4.9$ magnetic field line from 220 km altitude to the equator.

It consists of three parts: (1) a linear density variation between the E and F regions, (2) an exponential density decrease at altitudes above the F peak, and (3) an exponential density variation in the magnetosphere. The scaling constants r_0, r_1, r_2, a_1, a_2, b_1, b_2, and γ should be assumed before the experiment or defined from the observations conducted during the experiment.

[15] For example, frequency modulations shown in Figure 1 were calculated before the experiment using formula (14) from *Streltsov et al.* [2009] and assuming that the electron density in the E region (100 km altitude, $r_1 = 1 + 100/R_E$) above HAARP is 3×10^4 cm^{-3}, the density in the F region (320 km altitude, $r_2 = 1 + 320/R_E$) is 3×10^5 cm^{-3}, and the density in the equatorial magnetosphere at geocentric distance of 4.9 R_E can take one of the following values: 10, 50, 100, 200, 300, or 400 cm^{-3}.

[16] Upon running the experiment and collecting observations, it becomes possible to perform simulations using more well-defined parameters of the magnetospheric/ionospheric densities. In particular, the density at low altitudes can be identified from the digisonde at the HAARP facility. At time 22:45 UT on 16 March 2008, the density was determined to be 7.15×10^4 cm^{-3} ($f_{pe} \approx 2.4$ MHz) at an altitude of 100 km and 2.63×10^5 cm^{-3} ($f_{pe} \approx 4.6$ MHz) at an altitude of 220 km. These values determine $r_1 = 1 + 100/R_E$, $r_2 = 1 + 220/R_E$, $a_1 = 7.15 \times 10^4$ cm^{-3}, and $a_2 = 2.63 \times 10^5$ cm^{-3}. The digisonde shows that the density changes by a factor of 0.189 from 220 km to 420 km altitude, which defines $r_0 = 0.0188$. To define b_1, b_2, and γ, we use the one-hop magnetospheric propagation time of 1.4 and 1.9 kHz components of the signal observed in the conjugate region during the experiment. These propagation times were determined to be 2.900 s and 2.675 s, respectively. There are a number of studies where plasma density in the magnetosphere is defined from ULF/VLF wave observations on the ground and on satellites [*Denton et al.*, 2006; *Lichtenberger*, 2009]. The simplest formula for the distribution of plasma density in the magnetosphere is given by *Denton et al.* [2002]: $n = n_* (L/r)^\gamma$, where n_* is the reference density in the equatorial plane on L dipole magnetic shell, and $\gamma \approx 1$ inside the plasmasphere and $\gamma \approx 2.5$ outside the plasmasphere. To incorporate this formula into our model we define $b_2 = n_* L^\gamma$ (with $L = 4.9$) and $b_1 = a_2 - n_* (L/r_2)^\gamma$. We also assume $\gamma = 1$ and vary parameter n_* to match the traveling time for 1.4 and 1.9 kHz whistler waves observed in the experiment. This approach reveals that $n_* = 129$ cm^{-3} gives propagation times of 2.903 s for 1.4 kHz and 2.671 for 1.9 kHz, the values of which are quite close to the observations.

[17] Figure 4 shows profiles of the parallel wavelength, $\lambda_{\|} = 2\pi/k_{\|}$, and the parallel group velocity, $v_{\|g}$, defined by (6) of the whistler mode waves with frequencies 0.5, 1.0, 1.5, 2.0, and 2.5 kHz calculated from (1) and (2) along the $L = 4.9$ magnetic field line assuming dipole magnetic field and the background plasma density defined by (10) with parameters defined above.

5. Numerical Technique

[18] Equations (7)–(9) have been solved numerically as described by *Streltsov et al.* [2009] by using the finite difference time domain (FDTD) technique inside the 1D simulation domain, representing $L = 4.9$ dipole magnetic field line. In particular, partial derivatives in space were approximated with second-order finite differences, and a third-order predictor-corrector algorithm was used to advance equation (7) in time: The four-step Adams-Bashforth method was used as a predictor, and the three-step Adams-Moulton method was used as a corrector [*Burden and Faires*, 2001].

[19] Waves were launched from one side of the domain by specifying the following boundary conditions for the electric field: $E_x(t) = E_0 \sin[\phi(t)]$ and $E_y(t) = E_0 \cos[\phi(t)]$, where E_0 is a constant and $\phi(t) = 2\pi \int_0^t f(\tau) d\tau$, with $f(t)$ shown in Figure 1. At the other side of the domain we set $E_x(t) \equiv E_y(t) \equiv 0$, which correspond to a perfectly conducting ionosphere. One important feature of the 1D case considered in this study is that the model (7)–(9) becomes linear, which means that all nonlinear terms in equation (9) disappear, when the whistler mode wave propagates exactly along the ambient magnetic field [*Streltsov et al.*, 2009]. The linear nature of the problem makes the choice of the initial amplitude of the wave, E_0, quite arbitrary, and without further discussions we set it equal to 1 mV/m.

[20] Figure 4 shows that for realistic parameters of the Earth's magnetosphere, $\lambda_{\|}$ of whistler mode waves with frequencies from 0.5 to 2.5 kHz, strongly decreases near the

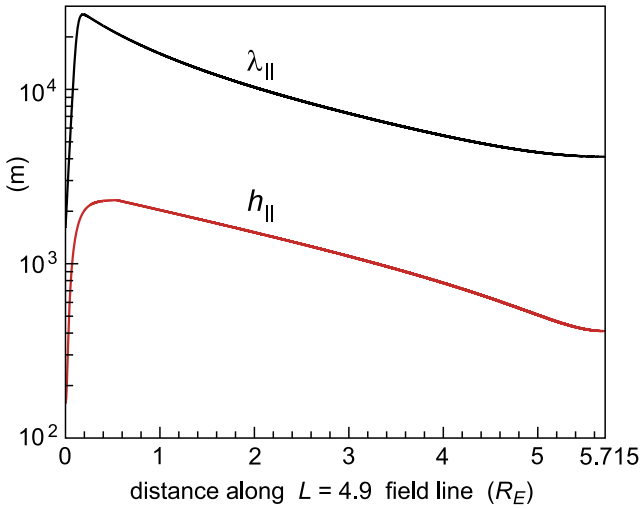

Figure 5. Parallel wavelength $\lambda_{||}$, of 2.5 kHz whistler mode wave and the size of the parallel discretization of the computational domain, $h_{||}$, along $L = 4.9$ magnetic field line from 220 km altitude to the equator.

ionosphere and in the equatorial magnetosphere. To accommodate this feature of the solution, the computational domain has been discretized with strongly nonuniform grids. Figure 5 shows plots of the parallel wavelength of 2.5 kHz whistler mode wave and the distance between two neighboring computational nodes used in the simulations along $L = 4.9$ magnetic field line. The grid used to calculate the wave electric field contains 100,001 nodes, and it is shifted by half of the distance between adjacent nodes from the grid used to calculate the wave magnetic field and the electron velocity. Because the predictor-corrector method used in this study belongs to the "time explicit" class of methods, it requires a very small step in time to be numerically stable. (In the time-explicit algorithms the time step and the distance between nodes should satisfy the so-called Courant-Friedrichs-Lewy condition [*Smith*, 1978].) Therefore, the small parallel wavelength of the whistler mode wave requires a high spatial resolution, which in turn requires a small time step to advance the solution in time, making the entire problem very computationally demanding.

[21] The way this problem has been solved is to run a simulation at a different moment in time not in the entire domain but only inside a subdomain, where the wave is dwelling during this time. For example, Figure 6 shows variations of the amplitude of y component of electric (left) and magnetic (right) fields, in simulations of the propagation of a whistler mode wave with a type 3 frequency modulation. These simulations were performed only inside subdomains where the wave dwells at this particular moment of time. For example, during the period of time from 2.86 to 3.13 s, the simulations were performed only inside a subdomain from 6.60 to 7.43 R_E (just south of the magnetic equator), discretized with 27,267 grid points. In this case, a simulation of the wave propagation along the $L = 4.9$ dipole magnetic field line starting at an altitude of 220 km takes 52 h and 16 min to accomplish on Dell Blade M610 Linux server with two X5560 2.8GHz quad-core Xeonprocessors. For comparison, the straightforward simulation of the same case inside the entire computational domain at every time step takes more than 3 times longer (178 h and 44 min). In this paper we did not conduct any optimization studies of how code performance depends on the parameters (sizes) of these subdomains. We just show an example of how this simple

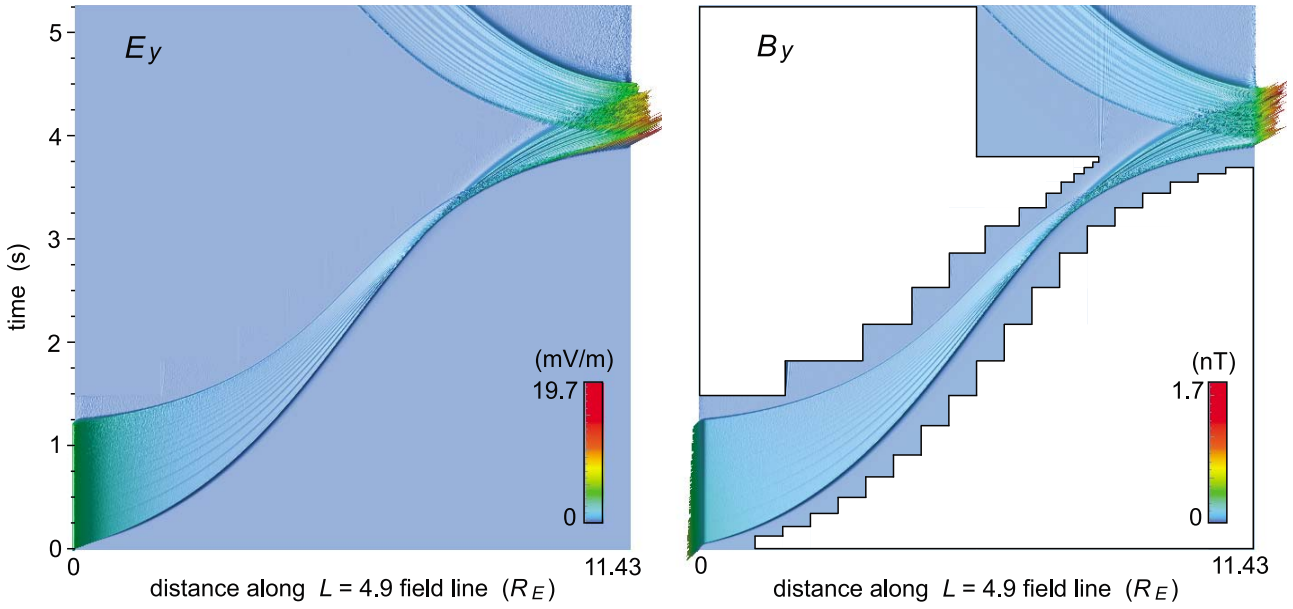

Figure 6. Variation of amplitude of E_y (left) and B_y (right) in the whistler mode wave with type 3 frequency modulation traveling along $L = 4.9$ magnetic field line. The right frame shows subdomains where the simulations have been performed in different moments of time.

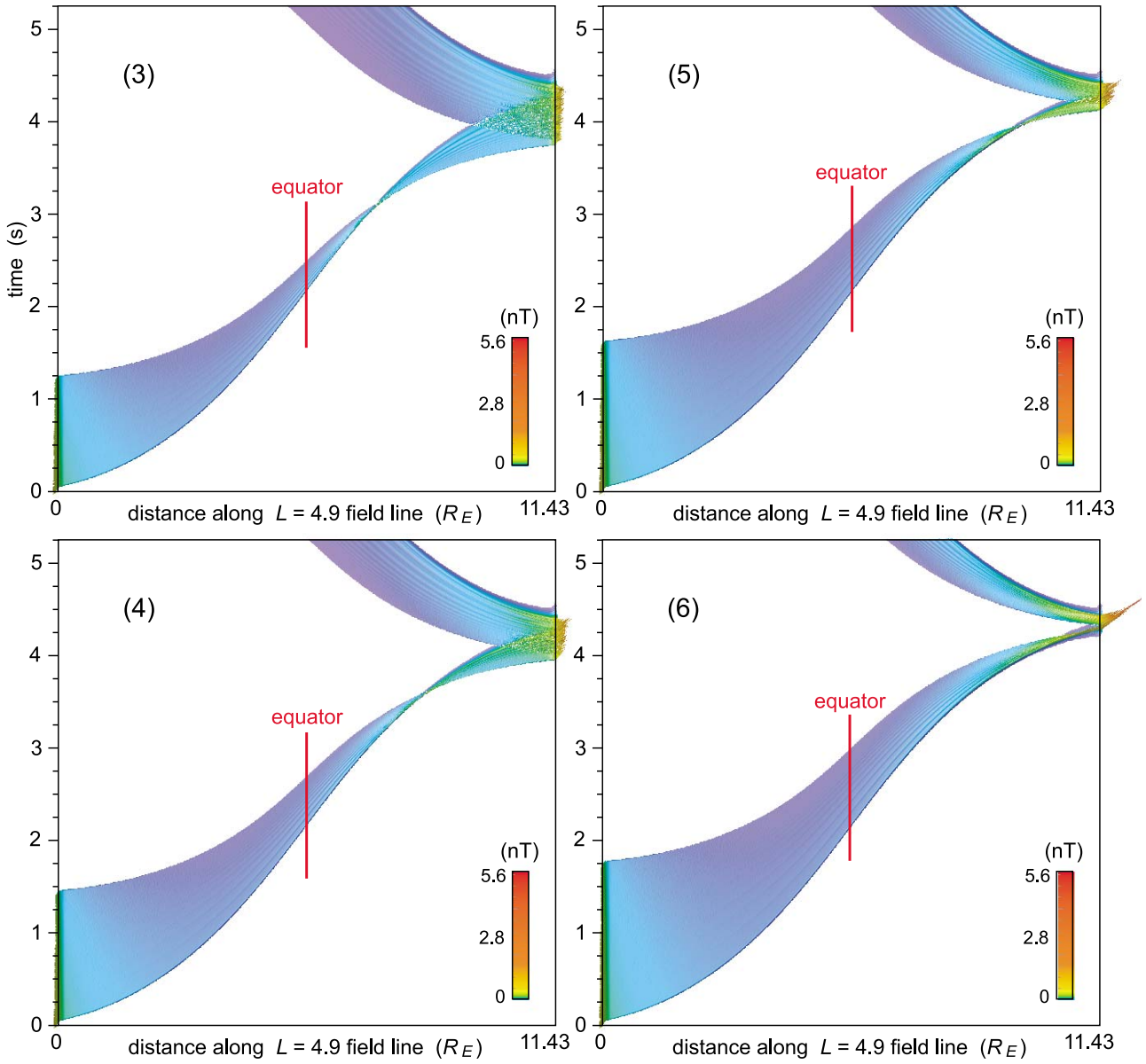

Figure 7. Variation of amplitude of B_y in whistler mode waves with frequency modulation of type 3, 4, 5, and 6 propagating along $L = 4.9$ magnetic field line.

technique can significantly (by a factor of 3) decrease the amount of simulations in this wave-propagation problem.

6. Results and Discussions

[22] Figure 7 shows variations of the amplitude of the y component of the magnetic field, B_y, in the whistler mode waves with frequency modulations of type 3, 4, 5, and 6, propagating along the $L = 4.9$ magnetic field line. Figure 8 shows the spectrogram of these signals taken at the left, "transmitting" (T) boundary of the domain (220 km altitude in the northern hemisphere); at the right, "receiving" (R) boundary (220 km altitude in the southern hemisphere); and in the middle of the domain corresponding to the equatorial magnetosphere (E). Figures 9 and 10 show the same quantities obtained in the simulations of the signals with frequency modulations of type 3′, 4′, 5′, and 6′.

[23] The first idea which we want to verify with these simulations is that the propagation time of 1.4 and 1.9 kHz frequency components of the frequency modulations of type 3′, 4′, 5′, and 6′, which were transmitted, are 2.9 s and 2.675 s. These intervals were estimated from the experimental data shown in Figure 3 for the signals with types 3′, 4′, 5′ frequency modulations. These time intervals were used to estimate the distribution of the plasma density in the magnetosphere used in the simulations. These time intervals are marked with black lines in Figure 10. The length of the linear segment marked with letters A and B is 2.9 s, and the length of the segment marked with letters C and D is 2.675 s. Figure 10 shows that these segments exactly

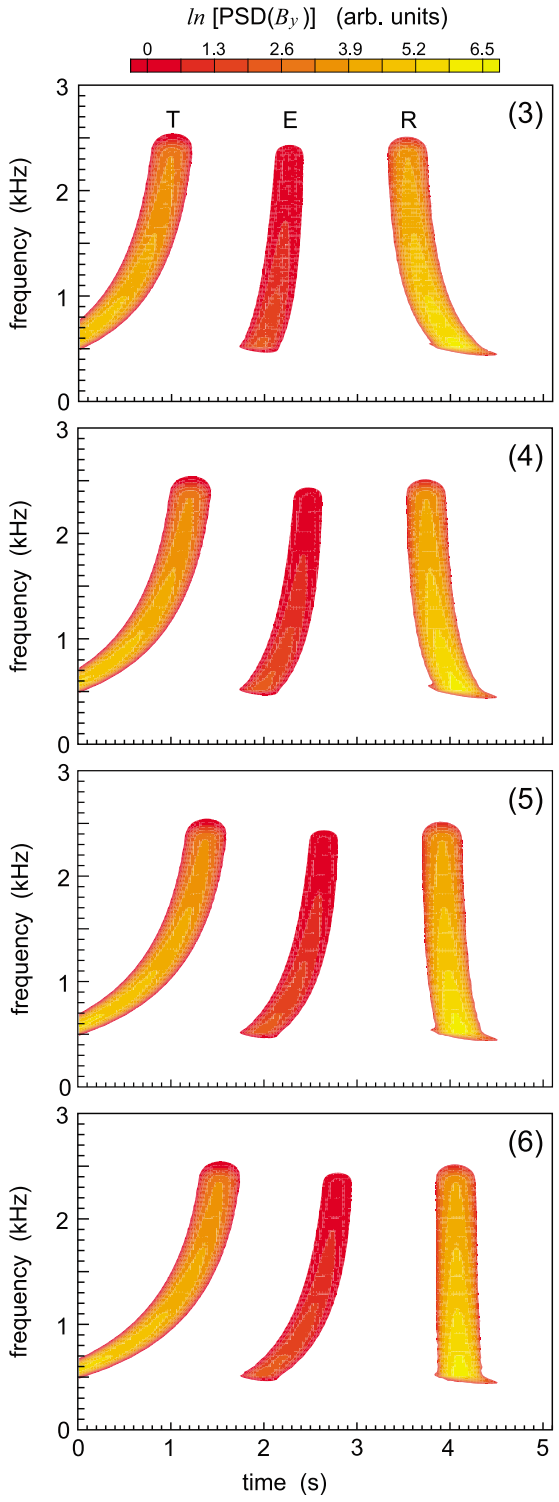

Figure 8. Spectrogram of the signal at the "transmitting" boundary of the domain (T); at the "receiving" boundary of the domain (R); and in the middle of the domain, near the equatorial plane (E) for whistler mode waves with frequency modulation of type 3, 4, 5, and 6 propagating along L = 4.9 magnetic field line.

connect the maximum in transmitted and received whistler mode waves with frequencies 1.4 and 1.9 kHz in all four signals with frequency modulations 3′, 4′, 5′, and 6′. There are two main conclusions from these results: One is that our model for the background density indeed represents a realistic density distribution in the magnetosphere and ionosphere during the HAARP experiment, and another is that our numerical algorithm adequately captures the basic physics of the propagation of the whistler mode waves in the magnetosphere.

[24] The experiment conducted at HAARP on 16 March 2008 demonstrates that none of the signals shown in Figures 7 and 8 (types 3, 4, 5, and 6) were amplified, but the signals shown in Figures 9 and 10 (types 3′, 4′, 5′, and 6′) were amplified. If we assume that the amplification occurs due to the interactions between whistler mode waves and energetic electrons in the equatorial magnetosphere [*Trakhtengerts et al.*, 2004, 2007; *Trakhtengerts and Rycroft*, 2008], then the main factor that defines amplification/non-amplification of the signal is the wave spectrogram measured at the equator (E). To make some quantitative conclusions about when this amplification will happen we introduce a linear rate,α (Figure 10), of the frequency modulation of the signal near the frequency 0.5 kHz (or in the frequency range from 0.5 to 1.0 kHz). This frequency interval is chosen because the observations shown in Figure 3 demonstrate that this frequency part of the signal is amplified more strongly than the higher-frequency part of the signal (from 1.0 to 2.5 kHz). A comparison between Figures 8 and 10 demonstrates that the amplification occurs when α is in the range from 0.25 to 0.47 kHz/s at the equator, and no amplification is detected when this rate is larger than 0.78 kHz/s (Figure 8, panel (6)). Figure 3 also shows that maximum amplification occurs when α = 0.33 kHz/s (Figure 10, panel (4′)), and no/very little amplification is observed when this gradient is equal to 0. (Two pulses with constant frequencies of 1250 and 1510 Hz were observed in the conjugate region and can be seen faintly around 39 and 44 s in the bottom panel of Figure 3, but their magnitudes are much smaller than the magnitude of the modulated signals.)

[25] The results from this experiment and from our numerical simulations are consistent with experiments conducted at Siple Station, Antarctica. In these earlier experiments, it was shown that signal amplification and triggering were not observed when two signals with a frequency difference less than 20 Hz were launched together, yet signals with a frequency difference of 100–200 Hz were amplified [*Carlson et al.*, 1985; *Helliwell*, 1988]. The mechanism causing this amplification of the monochromatic signals was called the coherent wave instability (CWI) [*Helliwell et al.*, 1980]. It suggests that true broadband signals are not amplified in the magnetosphere, and this situation can be avoided if the frequency of the transmitted wave changes not in a smooth, continuous format but rather in a discrete, "staircase-like" form with a step of 100–200 Hz [*Streltsov et al.*, 2009].

[26] Experiments at Siple Station also demonstrated several cases of amplification of signals with a linear frequency modulation (rising frequency) [*Mielke and Helliwell*, 1993] and signals with a frequency variation that have a positive slope but a negative curvature ("chirp"-like signals) [*Helliwell et al.*, 1990]. It was observed that these "chirp"-like signals amplify more rapidly than the signals with linear frequency variation. In our experiment, we observe ampli-

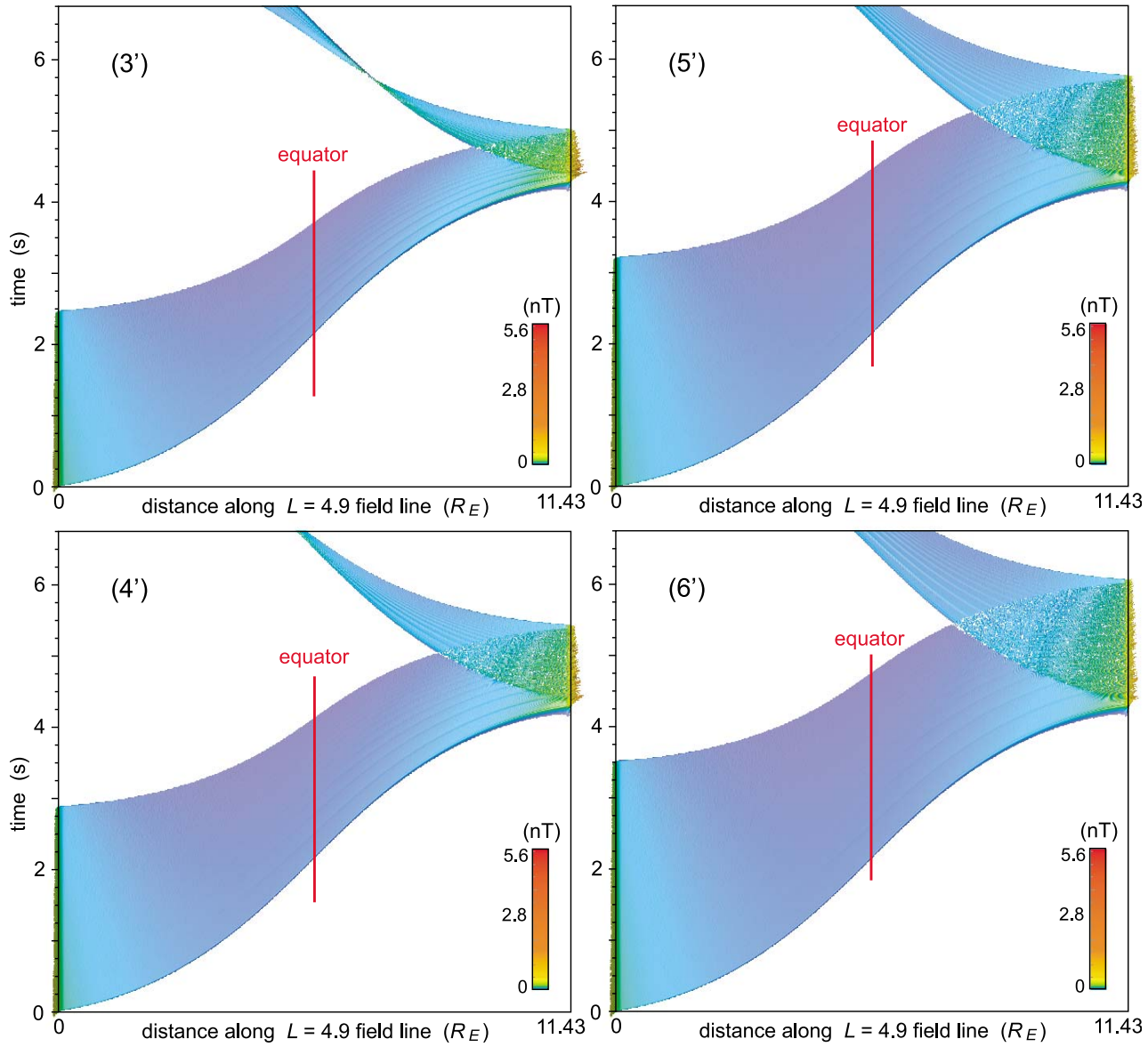

Figure 9. Variation of amplitude of B_y in whistler mode waves with frequency modulation of type 3′, 4′, 5′, and 6′ propagating along L = 4.9 magnetic field line.

fication of the signal with a positive frequency slope and a positive curvature, which make results from the HAARP experiment different substantially from the previous observations at Siple. It is also important to keep in mind that the Siple transmitter injected ELF/VLF waves of much higher amplitude into the magnetosphere than the HAARP transmitter does. Since both amplitude and frequency-time format determine where along the field line energetic particles are trapped, it is not expected for the results from the two experiments to be the same in terms of the frequency-time format. The HAARP experiment probes conditions closer to the nonlinear amplification threshold [*Helliwell et al.*, 1980], where the rate of the frequency change with time can be a significant parameter. We plan to perform a rigorous investigation of this problem by including dynamics of the energetic electrons and wave-particle interactions in the next generation of the present model.

7. Conclusions

[27] Results from the experiment conducted at HAARP on 16 March 2008 demonstrate that whistler mode waves with a particular form of the frequency modulation can be amplified on their pass from the HAARP to the conjugate location in the southern Pacific Ocean more efficiently than the signal with a constant frequency. Because numerous theoretical studies suggest that this wave amplification occurs due to the interaction between this wave and energetic electrons in the equatorial magnetosphere, it is important to know wave parameters in this particular region.

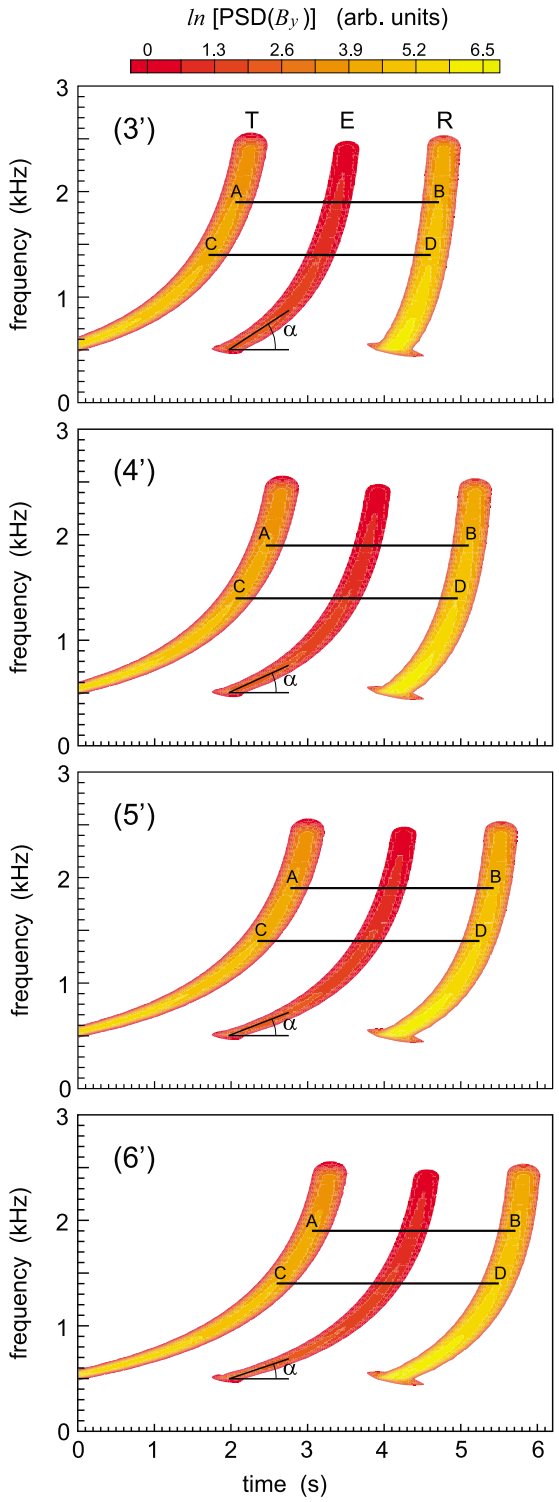

Figure 10. Spectrogram of the signal at the "transmitting" boundary of the domain (T); at the "receiving" boundary of the domain (R); and in the middle of the domain, near the equatorial plane (E) for whistler mode waves with frequency modulation of type 3′, 4′, 5′, and 6′ propagating along L = 4.9 magnetic field line.

Numerical simulations of EMHD equations in the dipole magnetic field geometry reveal that the amplification take place more efficiently when the frequency of the whistler mode waves (in the frequency range from 0.5 to 1.0 kHz) changes in the equatorial magnetosphere with the rate from 0.25 to 0.47 kHz/s. The maximum amplification occurs when this rate is 0.33 kHz/s, and no/very little amplification was observed when this gradient is equal to 0 or when it is larger than 0.78 kHz/s. The results from this study will be used in our future studies of the wave-particle interactions in the equatorial magnetosphere and for planning and explanation of future HAARP experiments.

[28] **Acknowledgments.** The High Frequency Active Auroral Research Program (HAARP) is a Department of Defense project operated jointly by the U.S. Air Force and U.S. Navy. This work is supported in part by the ONR MURI Award 528828 to the University of Maryland. The experiment at HAARP was conducted during a research campaign sponsored by the Air Force Research Laboratory. Authors thank Mike McCarrick and other HAARP personnel for help with the experiment. [29] Robert Lysak thanks Michael Rycroft and another reviewer for their assistance in evaluating this paper.

References

Angerami, J. (1970), Whistler duct properties deduced from VLF observations made with the OGO 3 satellite near the magnetic equator, *J. Geophys. Res.*, *75*, 6115–6135.

Burden, R., and J. Faires (2001), *Numerical Analysis*, 810 pp., Brooks/Cole, New York.

Carlson, C., R. Helliwell, and D. Carpenter (1985), Variable frequency VLF signals in the magnetosphere: Associated phenomena and plasma diagnostics, *J. Geophys. Res.*, *90*(A2), 1507–1521.

Carpenter, D., and R. Anderson (1992), An ISSE/whistler model of equatorial electron density in the magnetosphere, *J. Geophys. Res.*, *97*(A2), 1097–1108.

Cohen, M., M. Gołkowski, and U. Inan (2008), Orientation of the HAARP ELF ionospheric dipole and the auroral electrojet, *Geophys. Res. Lett.*, *35*, L02806, doi:10.1029/2007GL032424.

Cohen, M., U. Inan, and E. Paschal (2010), Sensitive broadband ELF/VLF radio reception with the AWESOME instrument, *IEEE Trans. Geosci. Remote Sens.*, *48*(1), 3–17, doi:10.1109/TGRS.2009.2028,334.

Denton, R., J. Goldstein, and J. Menietti (2002), Field line dependence of magnetospheric electron density, *Geophys. Res. Lett.*, *29*(24), 2205, doi:10.1029/2002GL015963.

Denton, R., K. Takahashi, I. Galkin, P. Nsumei, X. Huang, B. Reinisch, R. Anderson, M. Sleeper, and W. Hughes (2006), Distribution of density along magnetospheric field lines, *J. Geophys. Res.*, *111*, A04213, doi:10.1029/2005JA011414.

Gołkowski, M., U. Inan, A. Gibby, and M. Cohen (2008), Magnetospheric amplification and emission triggering by ELF/VLF waves injected by the 3.6 MW HAARP ionospheric heater, *J. Geophys. Res.*, *113*, A10201, doi:10.1029/2008JA013157.

Gołkowski, M., U. Inan, and M. Cohen (2009), Cross modulation of whistler mode and HF waves above the HAARP ionospheric heater, *Geophys. Res. Lett.*, *36*, L15103, doi:10.1029/2009GL039669.

Gołkowski, M., U. Inan, M. Cohen, and A. Gibby (2010), Amplitude and phase of nonlinear magnetospheric wave growth excited by the HAARP HF heater, *J. Geophys. Res.*, *115*, A00F04, doi:10.1029/2009JA014610.

Gordeev, A., A. Kingsep, and L. Rudakov (1994), Electron magnetohydrodynamics, *Phys. Rep.*, *243*, 215–315.

Helliwell, R. (1965), *Whistlers and Related Ionospheric Phenomena*, 349 pp., Stanford Univ. Press, Stanford, Calif.

Helliwell, R. (1988), VLF simulated experiments in the magnetosphere from Siple station, Antarctica, *Rev. Geophys.*, *26*(3), 551–558.

Helliwell, R., D. Carpenter, and T. Mielke (1980), Power threshold for growth of coherent VLF signals in the magnetosphere, *J. Geophys. Res.*, *85*(A7), 3360–3366.

Helliwell, R., T. Mielke, and U. Inan (1990), Rapid whistler-mode wave growth resulting from frequency-time curvature, *Geophys. Res. Lett.*, *17*(5), 599–602.

Hobara, Y., V. Trakhtengerts, A. Demekhov, and M. Hayakawa (2000), Formation of electron beams by interaction of a whistler wave packet with radiation belt electrons, *J. Atmos. Sol. Terr. Phys.*, *62*, 541–552.

Inan, U., H. Chang, R. Helliwell, W. Imhof, J. Reagan, and M. Walt (1985), Precipitation of radiation belt electrons by man-made waves: A comparison between theory and measurement, *J. Geophys. Res.*, *90* (A1), 359–369.

Inan, U., T. Bell, J. Bortnik, and J. Albert (2003), Controlled precipitation of radiation belt electrons, *J. Geophys. Res.*, *108*(A5), 1186, doi:10.1029/2002JA009580.

Inan, U., et al. (2004), Multi-hop whistler-mode ELF/VLF signals and triggred emissions excited by the HAARP HF heater, *Geophys. Res. Lett.*, *31*, L24805, doi:10.1029/2004GL021647.

Karpman, V., Y. Istomin, and D. Shklyar (1974), Nonlinear theory of a quasimonochromatic whistler mode packet in inhomogeneous plasma, *Plasma Phys.*, *16*, 685.

Koons, H. (1989), Observations of large-amplitude whistler mode wave ducts in the outer plasmasphere, *J. Geophys. Res.*, *94*(A11), 15,393–15,393.

Kostrov, A., A. Kudrin, L. Kurina, G. Luchinin, A. Shaykin, and T. Zaboronkova (2000), Whistlers in thermally generated ducts with enhanced plasma density: Excitation and propagation, *Phys. Scripta*, *62*, 51.

Lichtenberger, J. (2009), A new whistler inversion method, *J. Geophys. Res.*, *114*, A07222, doi:10.1029/2008JA013799.

Mielke, T., and R. Helliwell (1993), Siple Station, Antarctica, experiments on staircase frequency ramps as approximations to continuous ramps, *J. Geophys. Res.*, *98*(A3), 4053–4061.

Moullard, O., A. Masson, H. Laakso, M. Parrot, P. Décréau, O. Santolik, and M. Andre (2002), Density modulated whistler mode emissions observed near the plasmapause, *Geophys. Res. Lett.*, *29*(20), 1975, doi:10.1029/2002GL015101.

Nunn, D. (1974), A self-consistent theory of triggered VLF emissions, *Planet. Space Sci.*, *22*, 349.

Nunn, D., and A. Smith (1996), Numerical simulations of whistler-triggered VLF emissions observed in Antarctica, *J. Geophys. Res.*, *101*(A3), 5261–5277.

Omura, Y., D. Nunn, H. Matsumoto, and M. Rycroft (1991), A review of observational, theoretical and numerical studies of VLF triggered emissions, *J. Atmos. Sol. Terr. Phys.*, *53*, 351.

Papadopoulos, K., T. Wallace, M. McCarrick, G. M. Milikh, and X. Yang (2003), On the efficiency of ELF/VLF generation using HF heating of the auroral electrojet, *Plasma Phys. Rep.*, *29*, 561.

Sazhin, S. (1993), *Whistler-Mode Waves in a Hot Plasma*, 258 pp., Cambridge University Press, Cambridge.

Scarf, F., and C. Chapell (1973), An association of magnetospheric whistler dispersion characteristics with changes in local plasma density, *J. Geophys. Res.*, *78*(10), 1597–1602.

Smith, G. (1978), *Numerical Solution of Partial Differential Equations: Finite Difference Methods*, 304 pp., Oxford Univ. Press, New York.

Stenzel, R. (1976), Whistler wave propagation in a large magnetoplasma, *Phys. Fluids*, *19*, 857.

Streltsov, A., M. Gołkowski, U. Inan, and K. Papadopoulos (2009), Effect of frequency modulation on whistler-mode waves in the magnetosphere, *J. Geophys. Res.*, *114*, A08214, doi:10.1029/2009JA014155.

Trakhtengerts, V., and M. Rycroft (2008), *Whistler and Alfvén Mode Cyclotron Masers in Space*, 346 pp., Cambridge Univ. Press, Cambridge, UK.

Trakhtengerts, V., M. Rycroft, and A. Demekhov (1996), Interaction of noise-like and discrete ELF/VLF emissions generated by cyclotron interactions, *J. Geophys. Res.*, *101*(A6), 13,293–13,301.

Trakhtengerts, V., A. Demekhov, E. Titova, B. Kozelov, O. Santolik, D. Gurnett, and M. Parrot (2004), Interpretation of Cluster data on chorus emissions using the backward wave oscillator model, *Phys. Plasmas*, *11*, 1345–1351.

Trakhtengerts, V., et al. (2007), Formation of VLF chorus frequency spectrum: Cluster data and comparison with the backward wave oscillator model, *Geophys. Res. Lett.*, *34*, L02104, doi:10.1029/2006GL027953.

M. Gołkowski, Department of Electrical Engineering, University of Colorado Denver, Campus Box 110, P. O. Box 173364 Denver, CO 80217-3364, USA. (mark.golkowski@ucdenver.edu)

U. S. Inan, Stanford University, 350 Serra Mall, Stanford, CA 94305, USA. (inan@stanford.edu)

K. D. Papadopoulos, Department of Physics and Astronomy, University of Maryland, College Park, MD 20742, USA. (dpapadop@umd.edu)

A. V. Streltsov, Thayer School of Engineering, Dartmouth College, 8000 Cummings Hall, Hanover, NH 03755, USA. (streltsov@dartmouth.edu)